

# DBLP: Noise Bridge Consistency Distillation For Efficient And Reliable Adversarial Purification

Chihan Huang<sup>1</sup>, Belal Alsinglawi<sup>2,\*</sup>, Islam Al-qudah<sup>3</sup>

<sup>1</sup>Nanjing University of Science and Technology

<sup>2</sup>Zayed University

<sup>3</sup>Higher Colleges of Technology

huangchihan@njjust.edu.cn, belal.alsinglawi@zu.ac.ae, ialqudah@hct.ac.ae

## Abstract

Recent advances in deep neural networks (DNNs) have led to remarkable success across a wide range of tasks. However, their susceptibility to adversarial perturbations remains a critical vulnerability. Existing diffusion-based adversarial purification methods often require intensive iterative denoising, severely limiting their practical deployment. In this paper, we propose Diffusion Bridge Distillation for Purification (DBLP), a novel and efficient diffusion-based framework for adversarial purification. Central to our approach is a new objective, noise bridge distillation, which constructs a principled alignment between the adversarial noise distribution and the clean data distribution within a latent consistency model (LCM). To further enhance semantic fidelity, we introduce adaptive semantic enhancement, which fuses multi-scale pyramid edge maps as conditioning input to guide the purification process. Extensive experiments across multiple datasets demonstrate that DBLP achieves state-of-the-art (SOTA) robust accuracy, superior image quality, and around 0.2s inference time, marking a significant step toward real-time adversarial purification.

## Introduction

Deep neural networks (DNNs) have achieved remarkable success across a wide range of tasks in recent years. However, their widespread deployment has raised increasing concerns about their security and robustness (He et al. 2016; Liu et al. 2021). It is now well-established that DNNs are highly vulnerable to adversarial attacks (Szegedy et al. 2014a), wherein imperceptible, carefully crafted perturbations are added to clean inputs to generate adversarial examples that can mislead the model into producing incorrect outputs (Huang and Shen 2025).

To address this issue, adversarial training (AT) (Madry et al. 2019) has been proposed, which retrains classifiers using adversarial examples. However, AT suffers from high computational cost and poor generalization to unseen threats, limiting its applicability in real-world adversarial defense scenarios.

In contrast, adversarial purification (AP) has emerged as a compelling alternative due to its plug-and-play nature—requiring no retraining of the classifier—and its

stronger generalization capabilities. AP methods utilize generative models as a preprocessing step to transform adversarial examples into purified ones, which are then fed into the classifier for accurate predictions. The recent advances in diffusion models (Ho, Jain, and Abbeel 2020) have further propelled the development of AP. These models learn to transform simple distributions into complex data distributions through a forward noising and reverse denoising process. Crucially, this iterative denoising mechanism aligns well with the goal of removing adversarial perturbations, making diffusion models a natural fit for AP tasks (Nie et al. 2022).

However, existing diffusion-based purification approaches suffer from a critical limitation: they require multiple iterative denoising steps, resulting in prohibitively slow inference, which severely restricts their use in latency-sensitive applications such as autonomous driving (Chi et al. 2024) and industrial manufacturing (Wang et al. 2025). Moreover, most of these methods rely on a key assumption that the distributions of clean and adversarial samples converge after a certain number of forward diffusion steps. This allows the use of pretrained diffusion models, originally designed for generative tasks, to purify adversarial samples. However, this assumption only holds when the diffusion time horizon is sufficiently large. Empirical evidence from DiffPure suggests that excessive diffusion steps can lead to significant loss of semantic content, rendering accurate reconstruction of clean images infeasible.

In this paper, we propose Diffusion Bridge Distillation for Purification (DBLP), a novel framework designed to simultaneously address the two key limitations of existing diffusion-based adversarial purification methods: low inference efficiency and detail degradation. At its core, DBLP introduces a noise-bridged alignment strategy within the Latent Consistency Model (Luo et al. 2023a), effectively bridging adversarial noise and clean targets during the consistency distillation process to better align with the purification objective. By leveraging noise bridge distillation, DBLP enables direct recovery of clean samples from diffused adversarial inputs using an ODE solver. To further mitigate detail loss caused by fewer denoising steps, we introduce adaptive semantic enhancement, a lightweight yet effective conditioning mechanism that utilizes multi-scale pyramid edge maps to capture fine-grained structural features. These se-

semantic priors are injected into inference to enhance content preservation. DBLP achieves SOTA robust accuracy across multiple benchmark datasets while substantially reducing inference latency, requiring only 0.1 seconds per sample, thus making real-time adversarial purification feasible without compromising visual quality.

In summary, our contributions can be summarized as follows:

- We propose DBLP, a novel diffusion-based adversarial purification framework that significantly accelerates inference while preserving high visual quality and improving purification performance.
- We introduce a noise bridge distillation objective tailored for adversarial purification within the latent consistency model, effectively setting a bridge between adversarial noise and clean samples. Additionally, we design an adaptive semantic enhancement module that improves the model’s ability to retain fine-grained image details during purification.
- Comprehensive experiments across multiple benchmark datasets demonstrate that our method achieves SOTA performance in terms of robust accuracy, inference efficiency, and image quality, moving the field closer to practical real-time adversarial purification systems.

## Related Work

### Adversarial Training

Adversarial training is a prominent defense strategy against adversarial attacks (Goodfellow, Shlens, and Szegedy 2015), which enhances model robustness by retraining the model on perturbed adversarial examples (Lau et al. 2023). A substantial body of research has demonstrated its efficacy in adversarial defense. Notable methods include min-max optimization framework (Madry et al. 2018), TRADES which balances robustness and accuracy via a regularized loss (Zhang et al. 2019), and techniques like local linearization (Qin et al. 2019) and mutual information optimization (Zhou et al. 2022). Despite its strong robustness, adversarial training suffers from several notable drawbacks. It often generalizes poorly to unseen attacks (Laidlaw, Singla, and Feizi 2021), and it incurs significant computational overhead due to the necessity of retraining the entire model. Moreover, it typically leads to a degradation in clean accuracy (Wong, Rice, and Kolter 2020).

### Adversarial Purification

Adversarial purification represents an alternative and effective defense strategy against adversarial attacks that circumvents the need for retraining the model. The core idea is to employ generative models to pre-process adversarially perturbed images, yielding purified versions that are subsequently fed into the classifier. Early efforts in this domain leveraged GANs (Samangouei, Kabkab, and Chellappa 2018) or score-based matching techniques (Yoon, Hwang, and Lee 2021; Song et al. 2021) to successfully restore adversarial images. DiffPure (Nie et al. 2022) advanced this with diffusion models, inspiring follow-ups like adversarially guided denoising (Wang et al. 2022; Wu, Ye,

and Gu 2022), improved evaluation frameworks (Lee and Kim 2023), gradient-based purification (Zhang et al. 2023a), dual-phase guidance (Song et al. 2024), and adversarial diffusion bridges (Li et al. 2025). Despite their promising results, these methods exhibit certain limitations. Many approaches rely on auxiliary classifiers, which often compromise generalization performance. Others involve iterative inference procedures that are computationally intensive and time-consuming, thereby limiting their practicality in real-time or resource-constrained scenarios.

### Diffusion Models

Diffusion models (Ho, Jain, and Abbeel 2020), originally introduced to enhance image generation capabilities, have since demonstrated remarkable success across various domains, including video synthesis (Ho et al. 2022) and 3D content generation (Luo and Hu 2021). As a class of score-based generative models, diffusion models operate by progressively corrupting images with Gaussian noise in the forward process, and subsequently generating samples by denoising in the reverse process (Huang and Tang 2025). Given a pre-defined forward trajectory  $\{\mathbf{x}_t\}_{t \in [0, T]}$ , indexed by a continuous time variable  $t$ , the forward process can be effectively modeled using a widely adopted stochastic differential equation (SDE) (Karras et al. 2022):

$$d\mathbf{x}_t = \boldsymbol{\mu}(\mathbf{x}_t, t)dt + \sigma(t)d\mathbf{w}_t, \quad (1)$$

where  $\boldsymbol{\mu}(\mathbf{x}_t, t)$  and  $\sigma(t)$  denote the drift and diffusion coefficients, respectively, while  $\{\mathbf{w}_t\}_{t \in [0, T]}$  represents a standard  $d$ -dimensional Brownian motion. Let  $p_t(\mathbf{x})$  denote the marginal distribution of  $\mathbf{x}_t$  at time  $t$ , and  $p_{\text{data}}(\mathbf{x})$  represent the distribution of the original data, then  $p_0(\mathbf{x}) = p_{\text{data}}(\mathbf{x})$ .

Remarkably, (Song et al. 2021) established the existence of an ordinary differential equation (ODE), referred to as the *Probability Flow* (PF) ODE, whose solution trajectories share the same marginal probability densities  $p_t(\mathbf{x})$  as those of the forward SDE:

$$d\mathbf{x}_t = \left[ \boldsymbol{\mu}(\mathbf{x}_t, t) - \frac{1}{2}\sigma(t)^2\nabla \log p_t(\mathbf{x}_t) \right] dt. \quad (2)$$

For sampling, a score model  $s_\phi(\mathbf{x}, t) \approx \nabla \log p_t(\mathbf{x})$  is first trained via score matching to approximate the gradient of the log-density at each time step. This learned score function is then substituted into Equation (2) to obtain an empirical estimate of the PF ODE:

$$\frac{d\mathbf{x}_t}{dt} = \boldsymbol{\mu}(\mathbf{x}_t, t) \mathbf{x}_t - \frac{1}{2}\sigma(t)^2 s_\phi(\mathbf{x}_t, t). \quad (3)$$

## Preliminaries

### Problem Formulation

Adversarial attacks were first introduced by (Szegedy et al. 2014b), who revealed the inherent vulnerability of neural networks to carefully crafted perturbations. An adversarial example  $\mathbf{x}_{\text{adv}}$  is visually and numerically close to a clean input  $\mathbf{x}$ , yet it is deliberately designed to mislead a classifier  $C$  into assigning it to an incorrect label, rather than the true class  $y_{\text{true}}$ , formally expressed as:

$$\arg \max_y C(y|\mathbf{x}_{\text{adv}}) \neq y_{\text{true}}, \quad (4)$$

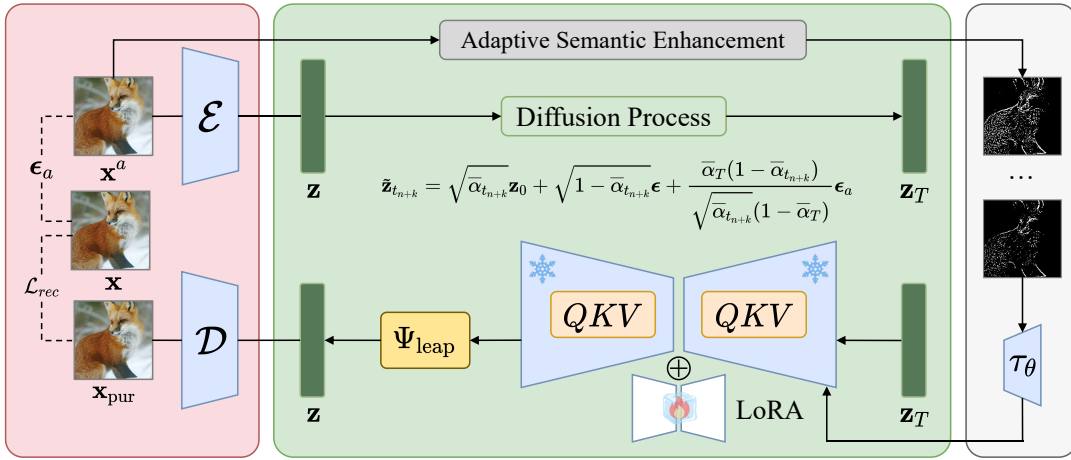


Figure 1: The overview structure of our DBLP. An adversary perturbs a clean image  $\mathbf{x}$  with noise  $\epsilon_a$  into an adversarial example  $\mathbf{x}^a$ , we first encode it into the latent space using the encoder  $\mathcal{E}$  to obtain the latent representation  $\mathbf{z}$ , followed by noise injection as defined in Equation (11). During training, we adopt a modified LCM-LoRA framework to perform noise bridge consistency distillation on the diffusion model, and employ a leapfrog ODE solver to accelerate sampling. During inference, we introduce adaptive semantic enhancement, using the weighted fusion of pyramid edge maps as a semantic-preserving condition to guide the purification process. The final purified image  $\mathbf{x}_{\text{pur}}$  is then recovered via the decoder  $\mathcal{D}$ .

with the constraint of  $\|\mathbf{x}_{\text{adv}} - \mathbf{x}\| \leq \epsilon$ , where  $\epsilon$  is the perturbation threshold.

The concept of adversarial purification is to transform the adversarial input  $\mathbf{x}_{\text{adv}}$  into a purified sample  $\mathbf{x}_{\text{pur}}$  before passing it to the classifier  $\mathcal{C}$ , such that  $\mathbf{x}_{\text{pur}}$  closely approximates the clean sample  $\mathbf{x}$  and yields the correct classification outcome. This process can be formulated as:

$$\max_{\mathbf{P}} \mathcal{C}(y_{\text{true}} | \mathbf{P}(\mathbf{x}_{\text{adv}})), \quad (5)$$

where  $\mathbf{P} : \mathbb{R}^d \rightarrow \mathbb{R}^d$  is the purification function.

### Consistency Models

The long inference time of diffusion models is a well-known limitation, prompting the introduction of the Consistency Model (Song et al. 2023), which enables the sampling process to be reduced to just a few steps, or even a single step. It proposes learning a direct mapping from any point  $\mathbf{x}_t$  along the PF ODE trajectory  $\{\mathbf{x}_t\}_{t \in [0, T]}$  back to its starting point, referred to as the consistency function, denoted as  $\mathbf{f} : (\mathbf{x}_t, t) \mapsto \mathbf{x}_\epsilon$ , where  $\mathbf{x}_\epsilon$  represents the starting state at a predefined small positive value  $\epsilon$ . The *self-consistency* property of this function can be formalized as:

$$\mathbf{f}(\mathbf{x}_t, t) = \mathbf{f}(\mathbf{x}_{t'}, t') \quad \forall t, t' \in [0, T]. \quad (6)$$

The goal of the consistency model  $\mathbf{f}_\theta$  is to estimate the underlying consistency function  $\mathbf{f}$  by enforcing the *self-consistency* property. The model  $\mathbf{f}_\theta$  can be parameterized as:

$$\mathbf{f}_\theta(\mathbf{x}, t) = c_{\text{skip}}(t)\mathbf{x} + c_{\text{out}}(t)F_\theta(\mathbf{x}, t), \quad (7)$$

where  $c_{\text{skip}}(t)$  and  $c_{\text{out}}(t)$  are differentiable functions. To satisfy the boundary condition  $\mathbf{f}(\mathbf{x}_\epsilon, \epsilon) = \mathbf{x}_\epsilon$ , we have  $c_{\text{skip}}(\epsilon) = 1$  and  $c_{\text{out}}(\epsilon) = 0$ .

Building on this, the Latent Consistency Model (Luo et al. 2023a) extends the consistency model to the latent space

using an auto-encoder (Rombach et al. 2022). In this setting, the consistency function conditioned on  $\mathbf{c}$  is defined as  $\mathbf{f}_\theta : (\mathbf{z}_t, \mathbf{c}, t) \mapsto \mathbf{z}_\epsilon$ . To fully leverage the capabilities of a pretrained text-to-image model, LCM parameterizes the consistency model as:

$$\mathbf{f}_\theta(\mathbf{z}, \mathbf{c}, t) = c_{\text{skip}}(t)\mathbf{z} + c_{\text{out}}(t) \left( \frac{\mathbf{z} - \sigma_t \hat{\epsilon}_\theta(\mathbf{z}, \mathbf{c}, t)}{\alpha_t} \right), \quad (8)$$

LCM-LoRA (Luo et al. 2023b) proposes distilling LCM using LoRA, significantly reducing the number of trainable parameters and thereby greatly decreasing training time and computational cost.

## Methodology

### Overall Framework

In this work, we aim to accelerate the purification backbone using a consistency distillation-inspired approach. Noting that the starting and ending points of the ODE trajectory respectively contain and exclude adversarial perturbations, we propose Noise Bridge Distillation in Section to explicitly align the purification objective.

To achieve acceleration, we leverage the Latent Consistency Model with LoRA-based distillation and introduce a leapfrog ODE solver for efficient sampling. During inference, as detailed in Section , we propose Adaptive Semantic Enhancement, which fuses pyramid edge maps into a semantic-preserving condition to guide the diffusion model toward effective purification.

### Noise Bridge Distillation

Following LCM (Luo et al. 2023a), let  $\mathcal{E}$  and  $\mathcal{D}$  denote the encoder and decoder that map images to and from the latent space, respectively. Given an image  $\mathbf{x}$ , its latent representation is  $\mathbf{z} = \mathcal{E}(\mathbf{x})$ . Unlike DDPM, DBLP includes adversarial

---

**Algorithm 1: Noise Bridge Distillation**


---

**Input:** Dataset  $\mathcal{D}$ , LCM  $\mathbf{f}_\theta$  and its initial model parameter  $\theta$ , classifier  $C$ , ground truth label  $y_{\text{true}}$ , Leapfrog ODE solver  $\Psi_{\text{leap}}$ , distance metric  $d(\cdot, \cdot)$ , EMA rate  $\mu$ , noise schedule  $\alpha_t$ , skip interval  $k$ , encoder  $\mathcal{E}$ ;  
 $\theta^- \leftarrow \theta$ ;  
1: **while** not convergence **do**  
2:   Sample  $\mathbf{x} \sim \mathcal{D}, n \sim \mathcal{U}[1, N - k]$ ;  
3:    $\mathbf{z} = \mathcal{E}(\mathbf{x})$ ;  
4:    $\epsilon_a = \arg \max_{\epsilon} \mathcal{L}(C(\mathcal{D}(\mathbf{z} + \epsilon)), y_{\text{true}})$ ;  
5:    $\tilde{\mathbf{z}}_{t_{n+k}}$   
6:    $= \sqrt{\bar{\alpha}_{t_{n+k}}} \mathbf{z}_0 + \sqrt{1 - \bar{\alpha}_{t_{n+k}}} \epsilon + \frac{\bar{\alpha}_T(1 - \bar{\alpha}_{t_{n+k}})}{\sqrt{\bar{\alpha}_{t_{n+k}}(1 - \bar{\alpha}_T)}} \epsilon_a$ ;  
7:    $\hat{\mathbf{z}}_{t_n}^{\Psi_{\text{leap}}} \leftarrow \mathbf{z}_{t_{n+k}} + \Psi(\mathbf{z}_{t_{n+k}}, t_{n+k}, t_n, \emptyset)$ ;  
8:    $\mathcal{L}_{\text{CD}}(\theta, \theta^-)$   
9:    $= d(\mathbf{f}_\theta(\tilde{\mathbf{z}}_{t_{n+k}}, \emptyset, t_{n+k}), \mathbf{f}_{\theta^-}(\hat{\mathbf{z}}_{t_n}^{\Psi_{\text{leap}}}, \emptyset, t_n))$ ;  
10:    $\mathcal{L}_{\text{rec}}(\theta) = d(\mathbf{f}_\theta(\tilde{\mathbf{z}}_t, \emptyset, t), \mathbf{z})$ ;  
11:    $\mathcal{L}(\theta, \theta^-) = \mathcal{L}_{\text{CD}}(\theta, \theta^-) + \lambda_{\text{rec}} \mathcal{L}_{\text{rec}}(\theta)$ ;  
12:    $\theta \leftarrow \theta - \eta \nabla_{\theta} \mathcal{L}(\theta, \theta^-)$ ;  
13:    $\theta^- \leftarrow \text{sg}(\mu \theta^- + (1 - \mu) \theta)$   
14: **end while**

---

perturbations  $\epsilon_a$  at the start of the noising process, such that  $\mathbf{z}_0^a = \mathbf{z}_0 + \epsilon_a$ . The perturbed forward process then becomes  $\mathbf{x}_t^a = \sqrt{\bar{\alpha}_t} \mathbf{x}_0^a + \sqrt{1 - \bar{\alpha}_t} \epsilon$ , where  $\epsilon \sim \mathcal{N}(\mathbf{0}, \mathbf{I})$ .

Our objective is to learn a trajectory that maps the diffused adversarial distribution ( $\mathbf{z}_T^a$ ) back to the clean data distribution ( $\mathbf{z}_0$ ). Notably, the starting point of this trajectory contains adversarial noise, whereas the endpoint does not. Therefore, we aim to find a consistency model  $\mathbf{f}_\theta$  that satisfies:  $\mathbf{f}_\theta(\mathbf{z}_t^a, \emptyset, t) = \mathbf{f}_\theta(\mathbf{z}_t, \emptyset, t) = \mathbf{z}_\epsilon$ , where  $\mathbf{z}_\epsilon \approx \mathbf{z}_0$  denotes the limiting state of  $\mathbf{z}_t$  as  $t \rightarrow 0$ . However, this contradicts Equation (7), as the trajectories initiated from  $\mathbf{z}_t$  and  $\mathbf{z}_t^a$  are misaligned, causing  $\mathbf{f}_\theta(\mathbf{z}_t^a, \emptyset, t) - \mathbf{f}_\theta(\mathbf{z}_t, \emptyset, t) \rightarrow \epsilon_a$ . To explicitly reconcile this discrepancy, we introduce a coefficient  $k_t$  and define an adjusted latent variable  $\tilde{\mathbf{x}}_t$  to align the trajectories accordingly:

$$\tilde{\mathbf{z}}_t = \mathbf{z}_t^a - k_t \epsilon_a, \quad (9)$$

with  $k_0 = 1$  and  $k_T = 0$ . Our goal is to ensure that the sampling distribution during the denoising process is independent of the adversarial perturbation  $\epsilon_a$ . Although  $\epsilon_a$  can be computed during training as  $\epsilon_a = \arg \max_{\epsilon} \mathcal{L}(C(\mathcal{D}(\mathbf{z} + \epsilon)), y_{\text{true}})$ , its exact value is unknown at inference time. Leveraging Bayes' theorem and the properties of Gaussian distributions, we achieve this by selecting the value of coefficient  $k_t$  such that the term involving  $\epsilon_a$  is eliminated. After a series of derivations, we obtain an explicit closed-form expression for  $k_t$ :

$$k_t = \sqrt{\bar{\alpha}_t} - \frac{\bar{\alpha}_T(1 - \bar{\alpha}_t)}{\sqrt{\bar{\alpha}_t(1 - \bar{\alpha}_T)}}, \quad 0 \leq t \leq T. \quad (10)$$

Thus the  $\tilde{\mathbf{z}}_t$  is constructed as:

$$\tilde{\mathbf{z}}_t = \sqrt{\bar{\alpha}_t} \mathbf{z}_0 + \sqrt{1 - \bar{\alpha}_t} \epsilon + \frac{\bar{\alpha}_T(1 - \bar{\alpha}_t)}{\sqrt{\bar{\alpha}_t(1 - \bar{\alpha}_T)}} \epsilon_a. \quad (11)$$

The full proof is provided in the Appendix.

Accordingly, based on the loss function introduced in LCM (Luo et al. 2023a), our consistency distillation loss can be formulated as:

$$\mathcal{L}_{\text{CD}}(\theta, \theta^-) = \mathbb{E}_{\mathbf{z}, n} [d(\mathbf{f}_\theta(\tilde{\mathbf{z}}_{t_{n+k}}, \emptyset, t_{n+k}), \mathbf{f}_{\theta^-}(\hat{\mathbf{z}}_{t_n}^{\Psi}, \emptyset, t_n))], \quad (12)$$

where  $d(\cdot, \cdot)$  denotes a distance metric, and  $\Psi(\cdot, \cdot, \cdot, \cdot)$  represents the DDIM (Song, Meng, and Ermon 2022) PF ODE solver  $\Psi_{\text{DDIM}}$ . The term  $\hat{\mathbf{z}}_{t_n}^{\Psi}$  refers to the solution estimated by the solver when integrating from  $t_{n+k}$  to  $t_n$ :

$$\hat{\mathbf{z}}_{t_n}^{\Psi} \leftarrow \mathbf{z}_{t_{n+k}} + \Psi(\mathbf{z}_{t_{n+k}}, t_{n+k}, t_n, \emptyset). \quad (13)$$

Following (Kim et al. 2024), we also incorporate a reconstruction-like loss that leverages clean images to better align the distillation training process with the purification objective:

$$\mathcal{L}_{\text{rec}}(\theta) = d(\mathbf{f}_\theta(\tilde{\mathbf{z}}_t, \emptyset, t), \mathbf{z}) \quad (14)$$

The training algorithm is detailed in Alg. 1.

**Leapfrog Solver** To enhance the dynamical interpretability of the sampling process, we refine the DDIM-based PF ODE solver using a leapfrog-inspired mechanism. Specifically, we decompose the prediction into a position-like estimate of the clean image and a velocity-like estimate of the noise, which are then updated jointly through a first-order leapfrog integration step (Verlet 1967):

$$\mathbf{z}_{t-1} = \mathbf{z}_0 + h \cdot \mathbf{v}_{1/2}, \quad (15)$$

where  $\mathbf{z}_0 = \sqrt{\bar{\alpha}_{t-1}} \hat{\mathbf{z}}_0$  represents the predicted clean image, while  $\mathbf{v}_0 = \sqrt{1 - \bar{\alpha}_{t-1}} \cdot \hat{\epsilon}$  serves as the midpoint velocity estimate.

### Adaptive Semantic Enhanced Purification

Although diffusion models are effective at learning the denoising process from noise to images, relying solely on this process often leads to the loss of fine-grained details (Berrada et al. 2025). While OSCP (Lei et al. 2025) attempts to mitigate this by incorporating edge maps to enhance structural information, it uses fixed-threshold Canny edge detection (Canny 1986), which lacks adaptability to varying attack intensities. Moreover, adversarial perturbations introduce noise that can interfere with accurate edge extraction. To address these issues, we propose Adaptive Semantic Enhancement, a non-trainable, computationally efficient module to aggregate multi-scale edge information, enhancing structural integrity and detail preservation.

Given an adversarial image  $\mathbf{x}_0^a \in \mathbb{R}^{H \times W \times 3}$ , we construct an  $L$ -level Gaussian blur pyramid and apply adaptive thresholding at each level  $l$  to compute the corresponding edge map:

$$\mathbf{E}_l = \text{Canny}(\text{GaussianBlur}(\mathbf{x}_0^a, \sigma_l)), \quad (16)$$

where the thresholds are calculated using Otsu (Otsu 1979) algorithm.

We employ a gradient-guided mechanism to fuse edge maps across different scales. We first upsample all edge

Architecture	Type	Method	Clean Acc.	Robuse Acc.			
				$\ell_\infty$	$\ell_1$	$\ell_2$	Avg.
WRN-70-16	—	Vanilla	96.36	0.00	0.00	0.00	0.00
WRN-70-16	AT	(Gowal et al. 2021a)	91.10	65.92	8.26	27.56	33.91
WRN-70-16		(Rebuffi et al. 2021)	88.54	64.26	12.06	32.29	36.20
WRN-70-16		Augment w/ Diff (Gowal et al. 2021b)	88.74	66.18	9.76	28.73	34.89
WRN-70-16		Augment w/ Diff (Wang et al. 2023)	93.25	70.72	8.48	28.98	36.06
MLP+WRN-28-10	AP	(Shi, Holtz, and Mishne 2021)	91.89	4.56	8.68	7.25	6.83
UNet+WRN-70-16		(Yoon, Hwang, and Lee 2021)	87.93	37.65	36.87	57.81	44.11
UNet+WRN-70-16		GDMP (Wang et al. 2022)	<u>93.16</u>	22.07	28.71	35.74	28.84
UNet+WRN-70-16		ScoreOpt (Zhang et al. 2023a)	91.41	13.28	10.94	28.91	17.71
UNet+WRN-70-16		Purify++ (Zhang et al. 2023b)	92.18	43.75	39.84	55.47	46.35
UNet+WRN-70-16		DiffPure (Nie et al. 2022)	92.50	42.20	44.30	60.80	49.10
UNet+WRN-70-16		ADBMs (Li et al. 2025)	91.90	47.70	49.60	63.30	53.50
UNet+WRN-70-16		DBLP (Ours)	<b>94.8</b>	<b>58.4</b>	<b>59.4</b>	<b>64.4</b>	<b>60.73</b>

Table 1: Clean Accuracy and Robust Accuracy (%) results on CIFAR-10. Avg. denotes the average robust accuracy across three types of attack threats, vanilla refers to models without any adversarial defense mechanism. The best results are **bolded**, and the second best results are underlined.

maps to a unified resolution  $\mathbf{E}_l$ , then use gradient consistency to compute the weights for each scale:

$$\mathbf{A}_l = \frac{\exp\left(-\|\nabla \mathbf{x}_0^a - \nabla \tilde{\mathbf{E}}_l\|_2 / T^*\right)}{\sum_{k=1}^L \exp\left(-\|\nabla \mathbf{x}_0^a - \nabla \tilde{\mathbf{E}}_k\|_2 / T^*\right)} \quad (17)$$

where  $T^*$  is the temperature parameter. Finally the fused edge map is:

$$\mathbf{E}_{\text{fused}} = \sum_{l=1}^L \mathbf{A}_l \odot \tilde{\mathbf{E}}_l \quad (18)$$

We then use  $\mathbf{E}_{\text{fused}}$  as a condition in the LCM, resulting in a semantically enhanced purified image.

## Experiments

### Experimental Settings

**Datasets** We conduct extensive experiments to validate the effectiveness and efficiency of our proposed method across several widely-used datasets, including CIFAR-10 (Krizhevsky et al. 2009), ImageNet (Deng et al. 2009), and CelebA (Liu et al. 2015). CIFAR-10 consists of 60,000 color images of size 32×32 across 10 object classes, representing general-purpose natural scenes. ImageNet is a large-scale visual database with over 14 million human-annotated images spanning more than 20,000 categories. CelebA contains over 200,000 celebrity face images, each annotated with 40 facial attributes and five landmark points.

**Training Settings** For our pretrained diffusion backbone, we use Stable Diffusion v1.5 (Rombach et al. 2022). The distillation process is trained for 20,000 iterations with a batch size of 4, a learning rate of 8e-6, and a 500-step warm-up schedule. For our leapfrog solver  $\Psi_{\text{leap}}$ , we set  $k = 20$  in Equation (13) and  $h = 0.8$  in Equation (15). During training, adversarial noise is generated using PGD-100 with  $\epsilon = 4/255$ , targeting a ResNet-50 (He et al. 2016) classifier.

Method	AF	FN	MFN
w/o Defense	0.0	0.3	0.0
GaussianBlur ( $\sigma = 7.0$ )	2.8	51.4	2.8
SHIELD (Das et al. 2018)	17.3	84.1	27.6
OSCP (Lei et al. 2025)	<b>86.8</b>	<u>97.8</u>	<u>84.9</u>
DBLP (Ours)	<u>82.4</u>	<b>98.8</b>	<b>91.0</b>

Table 2: Robust Accuracy (%) results on CelebA under PGD-10. The best results are **bolded**, and the second-best results are underlined.

**Evaluation Metrics** We evaluate our approach using multiple metrics: clean accuracy (performance on clean data), robust accuracy (performance under adversarial attack), inference time, and image quality metrics including LPIPS (Zhang et al. 2018), PSNR, and SSIM (Horé and Ziou 2010).

### Results

**CIFAR-10** We first conduct experiments on the CIFAR-10 dataset, evaluating our method under adversarial threats constrained by  $\ell_\infty$ ,  $\ell_1$ , and  $\ell_2$  norms. Since DBLP is trained under  $\ell_\infty$  attacks, this scenario is considered a seen threat, while the  $\ell_1$  and  $\ell_2$  settings are treated as unseen threats. The results are presented in Table 1. Although DBLP belongs to the category of adversarial purification methods, its access to the victim classifier makes it comparable to SOTA adversarial training and purification methods. Adversarial training performs well on seen threats but generalizes poorly to unseen ones, and DiffPure variants offer limited gains. In contrast, DBLP achieves substantially higher robust accuracy on both seen and unseen threats, while preserving strong clean accuracy. It outperforms prior methods by XXXX%, highlighting its robustness, generalization, and efficiency.

Method	Type	Attack	Standard Acc.	Robust Acc.	Architecture
w/o Defense	–	PGD-100	80.55	0.01	Res-50
(Schott et al. 2019)	AT	PGD-40	72.70	47.00	Res-152
(Wang et al. 2020)		PGD-100	53.83	28.04	Res-50
ConvStem (Singh et al. 2023)		AutoAttack	77.00	57.70	ConvNeXt-L
MeanSparse (Amini et al. 2024)		AutoAttack	77.96	59.64	ConvNeXt-L
DiffPure (Nie et al. 2022)	AP	PGD-100	68.22	42.88	Res-50
DiffPure (Nie et al. 2022)		AutoAttack	71.16	44.39	WRN-50-2
(Bai et al. 2024)		PGD-200 ( $\epsilon = 8/255$ )	70.41	41.70	Res-50
(Lee and Kim 2023)		PGD+EOT	70.74	42.15	Res-50
(Lin et al. 2025)		PGD+EOT	68.75	45.90	Res-50
(Zollicoffer et al. 2025)		PGD-200 ( $\epsilon = 8/255$ )	73.98	56.54	Res-50
MimicDiffusion (Song et al. 2024)		AutoAttack	66.92	61.53	Res-50
ScoreOpt (Zhang et al. 2023a)		Transfer-PGD	71.68	62.10	WRN-50-2
(Pei et al. 2025)		PGD-200 ( $\epsilon = 8/255$ )	77.15	65.04	Res-50
OSCP (Lei et al. 2025)		PGD-100	77.63	73.89	Res-50
DBLP (Ours)		PGD-100	<b>78.2</b>	<b>75.6</b>	Res-50
DBLP (Ours)	AutoAttack	<u>78.0</u>	<u>74.8</u>	Res-50	
DBLP (Ours)	PGD-200 ( $\epsilon = 8/255$ )	77.4	74.2	Res-50	

Table 3: Clean Accuracy and Robust Accuracy (%) results on ImageNet. The default setting for attack is  $\epsilon = 4/255$ . The best results are **bolded**, and the second best results are underlined.

Method	LPIPS↓	PSNR↑	SSIM↑
$\mathbf{x}_{adv}$	0.0975	26.17	0.7764
DiffPure (Nie et al. 2022)	0.2616	24.11	0.7155
OSCP (Lei et al. 2025)	0.2370	24.13	0.7343
DBLP (Ours)	<b>0.1012</b>	<b>26.03</b>	<b>0.7655</b>

Table 4: A quality comparison between the clean image  $\mathbf{x}$  and the purified image  $\mathbf{x}_{pur}$ . The  $\mathbf{x}_{adv}$  row reports the metrics between the purified and adversarial images. The best results are **bolded**.

**ImageNet** We further conducted comprehensive experiments on the ImageNet dataset, with results summarized in Table 3. Compared to CIFAR-10, adversarial purification methods on this larger-scale dataset can achieve standard accuracy comparable to or even surpassing that of adversarial training, while offering substantially higher robust accuracy. Notably, our method, DBLP, consistently achieves strong performance across various adversarial attacks. Under PGD-100, AutoAttack, and PGD-200 (with  $\epsilon = 8/255$ ), DBLP outperforms previous SOTA approaches by 1.14%, 0.64%, and 0.04% on average, respectively, in terms of both standard and robust accuracy. These results demonstrate the scalability, robustness, and general applicability of DBLP across datasets of different complexity and size.

**Celeb-A** We further validated the effectiveness of our method on a subset of the CelebA-HQ dataset by evaluating it against three representative victim models: ArcFace (AF) (Deng et al. 2019), FaceNet (FN) (Schroff, Kalenichenko, and Philbin 2015), and MobileFaceNet (MFN) (Chen et al.

Method	runtime (s)
GDMP (Wang et al. 2022)	~ 19
DiffPure (Nie et al. 2022)	~ 25
OSCP (Lei et al. 2025)	~ 0.8
DBLP (Ours)	~ <b>0.2</b>

Table 5: Inference time of purification models to purify one image. The best results are **bolded**.

2018). Leveraging model weights pretrained on ImageNet, we applied our purification framework to adversarial face images. As shown in Table 2, DBLP significantly enhances purification performance on facial data, demonstrating its robust generalization across image resolutions and domains.

### Transferability

We further evaluated DBLP under the Diff-PGD attack (Xue et al. 2023). The LCM was trained using PGD-generated adversarial noise on ResNet-50 and tested for transfer robustness across diverse architectures, including ResNet-50/152, WideResNet-50-2 (Zagoruyko and Komodakis 2016), ConvNeXt-B (Liu et al. 2022), ViT-B-16 (Kolesnikov et al. 2021), and Swin-B (Liu et al. 2021). As shown in Table 6, DBLP consistently outperforms prior SOTA methods under Diff-PGD-10, demonstrating strong cross-architecture robustness.

### Image Quality

Beyond correct classification, adversarial purification also seeks to maintain visual fidelity relative to the clean input. As shown in Table 4, DBLP achieves strong image quality

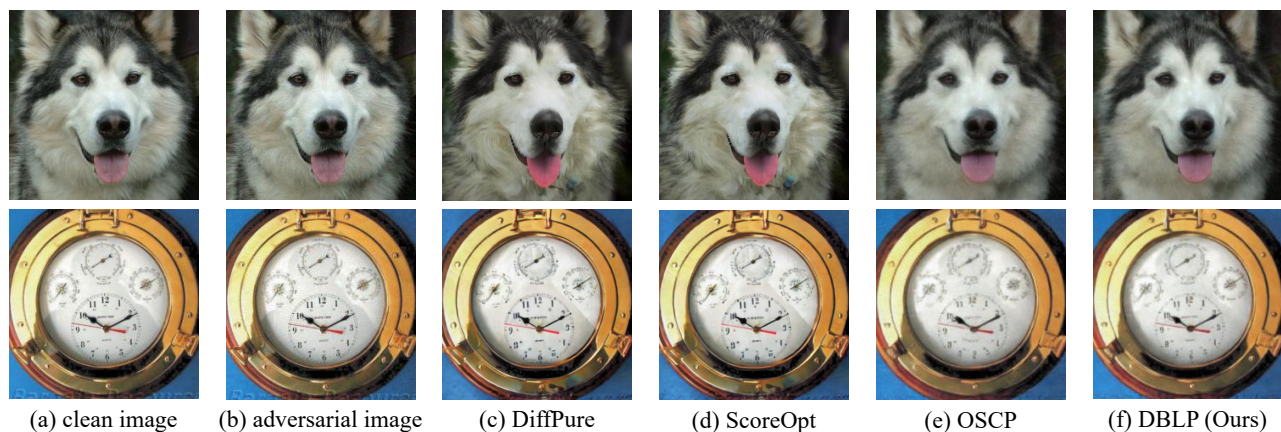


Figure 2: Visualization of (a) clean images, (b) adversarial images and (c-f) purified images under different method.

Method	ResNet-50	ResNet-152	WideResNet-50-2	ConvNeXt-B	ViT-B-16	Swin-B
DiffPure (Nie et al. 2022)	53.8	49.4	52.2	42.9	16.6	45.1
OSCP (Lei et al. 2025)	59.0	56.5	57.9	49.1	34.1	53.9
DBLP (Ours)	<b>63.0</b>	<b>59.4</b>	<b>60.7</b>	<b>52.4</b>	<b>38.2</b>	<b>58.3</b>

Table 6: Robust Accuracy (%) on DBLP under Diff-PGD-10 attack  $\epsilon = 8/255$  on ImageNet.

	Robust Acc.	LPIPS $\downarrow$	SSIM $\uparrow$
w/o Edge Map	74.2	0.1386	0.7409
Edge Map	74.8	0.1172	0.7430
Pyramid Edge Map	75.6	0.1012	0.7655

Table 7: Ablation study of adaptive semantic enhancement.

across all three metrics, with purified outputs  $x_{pur}$  closely matching both adversarial  $x_{adv}$  and clean images  $x$ . This highlights DBLP’s superior visual quality. Qualitative results in Figure 2 further confirm its ability to preserve fine-grained details.

### Inference Time

A key limitation of diffusion-based adversarial purification is the long inference time, which impedes real-time deployment. As shown in Table 5, DBLP achieves SOTA inference speed and significantly outperforms other methods. On ImageNet, it completes purification in just 0.2 seconds, greatly accelerating diffusion-based defenses and enabling practical real-time use.

### Ablation Study

We conduct ablation studies to assess the adaptive semantic enhancement module in DBLP, with results in Table 7. Omitting edge maps leads to a small drop in robust accuracy but a significant decline in image quality. Using pyramid edge maps further improves both metrics, showing that multi-scale edge representations better capture structural details and enhance visual fidelity. We further conduct a parameter analysis on the number of inference steps, as shown

in Figure 3. As the number of steps increases, robust accuracy shows a slight improvement, while sampling time grows significantly.

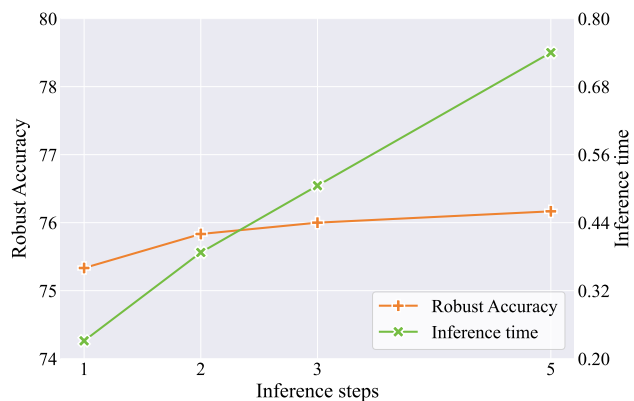


Figure 3: Parameter analysis of inference steps.

## Conclusion

In this work, we propose DBLP, an efficient diffusion-based adversarial purification framework. By introducing noise bridge distillation into the LCM, DBLP establishes a direct bridge between the adversarial and clean data distributions, significantly improving both robust accuracy and inference efficiency. Additionally, the adaptive semantic enhancement module fuses pyramid edge maps as conditional for LCM, leading to superior visual quality in purified images. Together, these advancements bring the scientific community closer to practical, real-time purification systems.

## Acknowledgments

This work was supported by the Innovalab.ai GPU research incentive for supporting research projects. Research Grant GPU-RTX2025.

## References

- Amini, S.; Teymoorianfard, M.; Ma, S.; and Houmansadr, A. 2024. MeanSparse: Post-Training Robustness Enhancement Through Mean-Centered Feature Sparsification. arXiv:2406.05927.
- Bai, M.; Huang, W.; Li, T.; Wang, A.; Gao, J.; Caiafa, C. F.; and Zhao, Q. 2024. Diffusion Models Demand Contrastive Guidance for Adversarial Purification to Advance. In Salakhutdinov, R.; Kolter, Z.; Heller, K.; Weller, A.; Oliver, N.; Scarlett, J.; and Berkenkamp, F., eds., *Proceedings of the 41st International Conference on Machine Learning*, volume 235 of *Proceedings of Machine Learning Research*, 2375–2391. PMLR.
- Berrada, T.; Astolfi, P.; Hall, M.; Havasi, M.; Benchetrit, Y.; Romero-Soriano, A.; Alahari, K.; Drozdal, M.; and Verbeek, J. 2025. Boosting Latent Diffusion with Perceptual Objectives. In *International Conference on Learning Representations*.
- Canny, J. 1986. A Computational Approach to Edge Detection. *IEEE Transactions on Pattern Analysis and Machine Intelligence*, PAMI-8(6): 679–698.
- Chen, S.; Liu, Y.; Gao, X.; and Han, Z. 2018. MobileFaceNets: Efficient CNNs for Accurate Real-Time Face Verification on Mobile Devices. 428–438.
- Chi, L.; Msahli, M.; Zhang, Q.; Qiu, H.; Zhang, T.; Memmi, G.; and Qiu, M. 2024. Adversarial Attacks on Autonomous Driving Systems in the Physical World: a Survey. *IEEE Transactions on Intelligent Vehicles*, 1–22.
- Das, N.; Shanbhogue, M.; Chen, S.-T.; Hohman, F.; Li, S.; Chen, L.; Kounavis, M. E.; and Chau, D. H. 2018. SHIELD: Fast, Practical Defense and Vaccination for Deep Learning using JPEG Compression. In *Proceedings of the 24th ACM SIGKDD International Conference on Knowledge Discovery & Data Mining*, KDD '18, 196–204. New York, NY, USA: Association for Computing Machinery. ISBN 9781450355520.
- Deng, J.; Dong, W.; Socher, R.; Li, L.-J.; Li, K.; and Fei-Fei, L. 2009. ImageNet: A large-scale hierarchical image database. In *2009 IEEE Conference on Computer Vision and Pattern Recognition*, 248–255.
- Deng, J.; Guo, J.; Xue, N.; and Zafeiriou, S. 2019. ArcFace: Additive Angular Margin Loss for Deep Face Recognition. In *Proceedings of the IEEE/CVF Conference on Computer Vision and Pattern Recognition (CVPR)*.
- Dhariwal, P.; and Nichol, A. 2021. Diffusion models beat GANs on image synthesis. In *Proceedings of the 35th International Conference on Neural Information Processing Systems*, NIPS '21. Red Hook, NY, USA: Curran Associates Inc. ISBN 9781713845393.
- Goodfellow, I.; Shlens, J.; and Szegedy, C. 2015. Explaining and Harnessing Adversarial Examples. In *International Conference on Learning Representations*.
- Gowal, S.; Qin, C.; Uesato, J.; Mann, T.; and Kohli, P. 2021a. Uncovering the Limits of Adversarial Training against Norm-Bounded Adversarial Examples. arXiv:2010.03593.
- Gowal, S.; Rebuffi, S.-A.; Wiles, O.; Stimberg, F.; Calian, D.; and Mann, T. 2021b. Improving robustness using generated data. In *Proceedings of the 35th International Conference on Neural Information Processing Systems*, NIPS '21. Red Hook, NY, USA: Curran Associates Inc. ISBN 9781713845393.
- He, K.; Zhang, X.; Ren, S.; and Sun, J. 2016. Deep Residual Learning for Image Recognition. In *2016 IEEE Conference on Computer Vision and Pattern Recognition (CVPR)*, 770–778.
- Ho, J.; Jain, A.; and Abbeel, P. 2020. Denoising diffusion probabilistic models. In *Proceedings of the 34th International Conference on Neural Information Processing Systems*, NIPS '20. Red Hook, NY, USA: Curran Associates Inc. ISBN 9781713829546.
- Ho, J.; Salimans, T.; Gritsenko, A.; Chan, W.; Norouzi, M.; and Fleet, D. J. 2022. Video Diffusion Models. In Koyejo, S.; Mohamed, S.; Agarwal, A.; Belgrave, D.; Cho, K.; and Oh, A., eds., *Advances in Neural Information Processing Systems*, volume 35, 8633–8646. Curran Associates, Inc.
- Horé, A.; and Ziou, D. 2010. Image Quality Metrics: PSNR vs. SSIM. In *2010 20th International Conference on Pattern Recognition*, 2366–2369.
- Huang, C.; and Shen, X. 2025. HUANG: A Robust Diffusion Model-based Targeted Adversarial Attack Against Deep Hashing Retrieval. *Proceedings of the AAAI Conference on Artificial Intelligence*, 39(4): 3626–3634.
- Huang, C.; and Tang, H. 2025. ScoreAdv: Score-based Targeted Generation of Natural Adversarial Examples via Diffusion Models. arXiv:2507.06078.
- Karras, T.; Aittala, M.; Aila, T.; and Laine, S. 2022. Elucidating the Design Space of Diffusion-Based Generative Models. In Koyejo, S.; Mohamed, S.; Agarwal, A.; Belgrave, D.; Cho, K.; and Oh, A., eds., *Advances in Neural Information Processing Systems*, volume 35, 26565–26577. Curran Associates, Inc.
- Kim, D.; Lai, C.-H.; Liao, W.-H.; Murata, N.; Takida, Y.; Uesaka, T.; He, Y.; Mitsufuji, Y.; and Ermon, S. 2024. Consistency Trajectory Models: Learning Probability Flow ODE Trajectory of Diffusion. In *International Conference on Learning Representations*.
- Kolesnikov, A.; Dosovitskiy, A.; Weissenborn, D.; Heigold, G.; Uszkoreit, J.; Beyer, L.; Minderer, M.; Dehghani, M.; Houtsby, N.; Gelly, S.; Unterthiner, T.; and Zhai, X. 2021. An Image is Worth 16x16 Words: Transformers for Image Recognition at Scale. In *International Conference on Learning Representations*.
- Krizhevsky, A.; et al. 2009. Learning multiple layers of features from tiny images. In *California Institute of Technology*.
- Laidlaw, C.; Singla, S.; and Feizi, S. 2021. Perceptual Adversarial Robustness: Defense Against Unseen Threat Models. In *International Conference on Learning Representations*.

- Lau, C. P.; Liu, J.; Souril, H.; Lin, W.-A.; Feizi, S.; and Chellappa, R. 2023. Interpolated Joint Space Adversarial Training for Robust and Generalizable Defenses. *IEEE Transactions on Pattern Analysis and Machine Intelligence*, 45(11): 13054–13067.
- Lee, M.; and Kim, D. 2023. Robust Evaluation of Diffusion-Based Adversarial Purification. In *Proceedings of the IEEE/CVF International Conference on Computer Vision (ICCV)*, 134–144.
- Lei, C. T.; Yam, H. M.; Guo, Z.; Qian, Y.; and Lau, C. P. 2025. Instant Adversarial Purification with Adversarial Consistency Distillation. In *Proceedings of the Computer Vision and Pattern Recognition Conference (CVPR)*, 24331–24340.
- Li, X.; Sun, W.; Chen, H.; Li, Q.; Liu, Y.; He, Y.; Shi, J.; and Hu, X. 2025. ADBM: Adversarial diffusion bridge model for reliable adversarial purification. In *International Conference on Learning Representations*.
- Lin, G.; Tao, Z.; Zhang, J.; Tanaka, T.; and Zhao, Q. 2025. Adversarial Guided Diffusion Models for Adversarial Purification. arXiv:2403.16067.
- Liu, Z.; Lin, Y.; Cao, Y.; Hu, H.; Wei, Y.; Zhang, Z.; Lin, S.; and Guo, B. 2021. Swin Transformer: Hierarchical Vision Transformer Using Shifted Windows. In *Proceedings of the IEEE/CVF International Conference on Computer Vision (ICCV)*, 10012–10022.
- Liu, Z.; Luo, P.; Wang, X.; and Tang, X. 2015. Deep Learning Face Attributes in the Wild. In *Proceedings of International Conference on Computer Vision (ICCV)*.
- Liu, Z.; Mao, H.; Wu, C.-Y.; Feichtenhofer, C.; Darrell, T.; and Xie, S. 2022. A ConvNet for the 2020s. In *2022 IEEE/CVF Conference on Computer Vision and Pattern Recognition (CVPR)*, 11966–11976.
- Luo, S.; and Hu, W. 2021. Diffusion Probabilistic Models for 3D Point Cloud Generation. In *Proceedings of the IEEE/CVF Conference on Computer Vision and Pattern Recognition (CVPR)*, 2837–2845.
- Luo, S.; Tan, Y.; Huang, L.; Li, J.; and Zhao, H. 2023a. Latent Consistency Models: Synthesizing High-Resolution Images with Few-Step Inference. arXiv:2310.04378.
- Luo, S.; Tan, Y.; Patil, S.; Gu, D.; von Platen, P.; Passos, A.; Huang, L.; Li, J.; and Zhao, H. 2023b. LCM-LoRA: A Universal Stable-Diffusion Acceleration Module. arXiv:2311.05556.
- Madry, A.; Makelov, A.; Schmidt, L.; Tsipras, D.; and Vladu, A. 2018. Towards Deep Learning Models Resistant to Adversarial Attacks. In *International Conference on Learning Representations*.
- Madry, A.; Makelov, A.; Schmidt, L.; Tsipras, D.; and Vladu, A. 2019. Towards Deep Learning Models Resistant to Adversarial Attacks. In *International Conference on Learning Representations*.
- Nie, W.; Guo, B.; Huang, Y.; Xiao, C.; Vahdat, A.; and Anandkumar, A. 2022. Diffusion Models for Adversarial Purification. In Chaudhuri, K.; Jegelka, S.; Song, L.; Szepesvari, C.; Niu, G.; and Sabato, S., eds., *Proceedings of the 39th International Conference on Machine Learning*, volume 162 of *Proceedings of Machine Learning Research*, 16805–16827. PMLR.
- Otsu, N. 1979. A Threshold Selection Method from Gray-Level Histograms. *IEEE Transactions on Systems, Man, and Cybernetics*, 9(1): 62–66.
- Pei, G.; Ma, K.; Sun, Y.; Xu, Q.; and Huang, Q. 2025. Diffusion-based Adversarial Purification from the Perspective of the Frequency Domain. arXiv:2505.01267.
- Qin, C.; Martens, J.; Gowal, S.; Krishnan, D.; Dvijotham, K. D.; Fawzi, A.; De, S.; Stanforth, R.; and Kohli, P. 2019. *Adversarial robustness through local linearization*. Red Hook, NY, USA: Curran Associates Inc.
- Rebuffi, S.-A.; Gowal, S.; Calian, D.; Stimberg, F.; Wiles, O.; and Mann, T. 2021. Data augmentation can improve robustness. In *Proceedings of the 35th International Conference on Neural Information Processing Systems, NIPS '21*. Red Hook, NY, USA: Curran Associates Inc. ISBN 9781713845393.
- Rombach, R.; Blattmann, A.; Lorenz, D.; Esser, P.; and Ommer, B. 2022. High-Resolution Image Synthesis With Latent Diffusion Models. In *Proceedings of the IEEE/CVF Conference on Computer Vision and Pattern Recognition (CVPR)*, 10684–10695.
- Samangouei, P.; Kabkab, M.; and Chellappa, R. 2018. Defense-GAN: Protecting Classifiers Against Adversarial Attacks Using Generative Models. In *International Conference on Learning Representations*.
- Schott, L.; Rauber, J.; Bethge, M.; and Brendel, W. 2019. Towards the first adversarially robust neural network model on MNIST. In *International Conference on Learning Representations*.
- Schroff, F.; Kalenichenko, D.; and Philbin, J. 2015. FaceNet: A unified embedding for face recognition and clustering. In *2015 IEEE Conference on Computer Vision and Pattern Recognition (CVPR)*, 815–823.
- Shi, C.; Holtz, C.; and Mishne, G. 2021. Online Adversarial Purification based on Self-Supervision. In *International Conference on Learning Representations*.
- Singh, N. D.; et al. 2023. Revisiting adversarial training for ImageNet: architectures, training and generalization across threat models. In *Proceedings of the 37th International Conference on Neural Information Processing Systems, NIPS '23*. Red Hook, NY, USA: Curran Associates Inc.
- Song, J.; Meng, C.; and Ermon, S. 2022. Denoising Diffusion Implicit Models. In *International Conference on Learning Representations*.
- Song, K.; Lai, H.; Pan, Y.; and Yin, J. 2024. MimicDiffusion: Purifying Adversarial Perturbation via Mimicking Clean Diffusion Model. In *Proceedings of the IEEE/CVF Conference on Computer Vision and Pattern Recognition (CVPR)*, 24665–24674.
- Song, Y.; Dhariwal, P.; Chen, M.; and Sutskever, I. 2023. Consistency Models. In Krause, A.; Brunskill, E.; Cho, K.; Engelhardt, B.; Sabato, S.; and Scarlett, J., eds., *Proceedings of the 40th International Conference on Machine Learning*,

- volume 202 of *Proceedings of Machine Learning Research*, 32211–32252. PMLR.
- Song, Y.; Sohl-Dickstein, J.; Kingma, D. P.; Kumar, A.; Ermon, S.; and Poole, B. 2021. Score-Based Generative Modeling through Stochastic Differential Equations. In *International Conference on Learning Representations*.
- Szegedy, C.; Zaremba, W.; Sutskever, I.; Bruna, J.; Erhan, D.; Goodfellow, I.; and Fergus, R. 2014a. Intriguing properties of neural networks. In *International Conference on Learning Representations*.
- Szegedy, C.; Zaremba, W.; Sutskever, I.; Bruna, J.; Erhan, D.; Goodfellow, I.; and Fergus, R. 2014b. Intriguing properties of neural networks. In *International Conference on Learning Representations*.
- Verlet, L. 1967. Computer "Experiments" on Classical Fluids. I. Thermodynamical Properties of Lennard-Jones Molecules. *Phys. Rev.*, 159: 98–103.
- Wang, H.; Wu, X.; Huang, Z.; and Xing, E. P. 2020. High-Frequency Component Helps Explain the Generalization of Convolutional Neural Networks. In *Proceedings of the IEEE/CVF Conference on Computer Vision and Pattern Recognition (CVPR)*.
- Wang, J.; Lyu, Z.; Lin, D.; Dai, B.; and Fu, H. 2022. Guided Diffusion Model for Adversarial Purification. arXiv:2205.14969.
- Wang, X.; Jiang, H.; Mu, M.; and Dong, Y. 2025. A trackable multi-domain collaborative generative adversarial network for rotating machinery fault diagnosis. *Mechanical Systems and Signal Processing*, 224: 111950.
- Wang, Z.; Pang, T.; Du, C.; Lin, M.; Liu, W.; and Yan, S. 2023. Better diffusion models further improve adversarial training. In *Proceedings of the 40th International Conference on Machine Learning, ICML'23*. JMLR.org.
- Wong, E.; Rice, L.; and Kolter, J. Z. 2020. Fast is better than free: Revisiting adversarial training. In *International Conference on Learning Representations*.
- Wu, Q.; Ye, H.; and Gu, Y. 2022. Guided Diffusion Model for Adversarial Purification from Random Noise. arXiv:2206.10875.
- Xue, H.; Araujo, A.; Hu, B.; and Chen, Y. 2023. Diffusion-Based Adversarial Sample Generation for Improved Stealthiness and Controllability. In Oh, A.; Naumann, T.; Globerson, A.; Saenko, K.; Hardt, M.; and Levine, S., eds., *Advances in Neural Information Processing Systems*, volume 36, 2894–2921. Curran Associates, Inc.
- Yoon, J.; Hwang, S. J.; and Lee, J. 2021. Adversarial Purification with Score-based Generative Models. In Meila, M.; and Zhang, T., eds., *Proceedings of the 38th International Conference on Machine Learning*, volume 139 of *Proceedings of Machine Learning Research*, 12062–12072. PMLR.
- Zagoruyko, S.; and Komodakis, N. 2016. Wide Residual Networks. In Richard C. Wilson, E. R. H.; and Smith, W. A. P., eds., *Proceedings of the British Machine Vision Conference (BMVC)*, 87.1–87.12. BMVA Press. ISBN 1-901725-59-6.
- Zhang, B.; et al. 2023a. Enhancing adversarial robustness via score-based optimization. In *Proceedings of the 37th International Conference on Neural Information Processing Systems, NIPS '23*. Red Hook, NY, USA: Curran Associates Inc.
- Zhang, B.; et al. 2023b. Purify++: Improving Diffusion-Purification with Advanced Diffusion Models and Control of Randomness. arXiv:2310.18762.
- Zhang, H.; Yu, Y.; Jiao, J.; Xing, E.; Ghaoui, L. E.; and Jordan, M. 2019. Theoretically Principled Trade-off between Robustness and Accuracy. In Chaudhuri, K.; and Salakhutdinov, R., eds., *Proceedings of the 36th International Conference on Machine Learning*, volume 97 of *Proceedings of Machine Learning Research*, 7472–7482. PMLR.
- Zhang, R.; Isola, P.; Efros, A. A.; Shechtman, E.; and Wang, O. 2018. The Unreasonable Effectiveness of Deep Features as a Perceptual Metric. In *Proceedings of the IEEE Conference on Computer Vision and Pattern Recognition (CVPR)*.
- Zhou, D.; Wang, N.; Gao, X.; Han, B.; Wang, X.; Zhan, Y.; and Liu, T. 2022. Improving Adversarial Robustness via Mutual Information Estimation. In Chaudhuri, K.; Jegelka, S.; Song, L.; Szepesvari, C.; Niu, G.; and Sabato, S., eds., *Proceedings of the 39th International Conference on Machine Learning*, volume 162 of *Proceedings of Machine Learning Research*, 27338–27352. PMLR.
- Zollicoffer, G.; Vu, M. N.; Nebgen, B.; Castorena, J.; Alexandrov, B.; and Bhattarai, M. 2025. LoRID: Low-Rank Iterative Diffusion for Adversarial Purification. *Proceedings of the AAAI Conference on Artificial Intelligence*, 39(21): 23081–23089.

# Reproducibility Checklist

## 1. General Paper Structure

- 1.1. Includes a conceptual outline and/or pseudocode description of AI methods introduced (yes/partial/no/NA) **yes**
- 1.2. Clearly delineates statements that are opinions, hypothesis, and speculation from objective facts and results (yes/no) **yes**
- 1.3. Provides well-marked pedagogical references for less-familiar readers to gain background necessary to replicate the paper (yes/no) **yes**

## 2. Theoretical Contributions

- 2.1. Does this paper make theoretical contributions? (yes/no) **yes**

If yes, please address the following points:

- 2.2. All assumptions and restrictions are stated clearly and formally (yes/partial/no) **yes**
- 2.3. All novel claims are stated formally (e.g., in theorem statements) (yes/partial/no) **yes**
- 2.4. Proofs of all novel claims are included (yes/partial/no) **yes**
- 2.5. Proof sketches or intuitions are given for complex and/or novel results (yes/partial/no) **yes**
- 2.6. Appropriate citations to theoretical tools used are given (yes/partial/no) **yes**
- 2.7. All theoretical claims are demonstrated empirically to hold (yes/partial/no/NA) **yes**
- 2.8. All experimental code used to eliminate or disprove claims is included (yes/no/NA) **NA**

## 3. Dataset Usage

- 3.1. Does this paper rely on one or more datasets? (yes/no) **yes**

If yes, please address the following points:

- 3.2. A motivation is given for why the experiments are conducted on the selected datasets (yes/partial/no/NA) **yes**
- 3.3. All novel datasets introduced in this paper are included in a data appendix (yes/partial/no/NA) **NA**
- 3.4. All novel datasets introduced in this paper will be made publicly available upon publication of the paper with a license that allows free usage for research purposes (yes/partial/no/NA) **NA**
- 3.5. All datasets drawn from the existing literature (potentially including authors' own previously pub-

lished work) are accompanied by appropriate citations (yes/no/NA) **yes**

- 3.6. All datasets drawn from the existing literature (potentially including authors' own previously published work) are publicly available (yes/partial/no/NA) **yes**

- 3.7. All datasets that are not publicly available are described in detail, with explanation why publicly available alternatives are not scientifically satisfying (yes/partial/no/NA) **NA**

## 4. Computational Experiments

- 4.1. Does this paper include computational experiments? (yes/no) **yes**

If yes, please address the following points:

- 4.2. This paper states the number and range of values tried per (hyper-) parameter during development of the paper, along with the criterion used for selecting the final parameter setting (yes/partial/no/NA) **yes**
- 4.3. Any code required for pre-processing data is included in the appendix (yes/partial/no) **no**
- 4.4. All source code required for conducting and analyzing the experiments is included in a code appendix (yes/partial/no) **no**
- 4.5. All source code required for conducting and analyzing the experiments will be made publicly available upon publication of the paper with a license that allows free usage for research purposes (yes/partial/no) **yes**
- 4.6. All source code implementing new methods have comments detailing the implementation, with references to the paper where each step comes from (yes/partial/no) **yes**
- 4.7. If an algorithm depends on randomness, then the method used for setting seeds is described in a way sufficient to allow replication of results (yes/partial/no/NA) **NA**
- 4.8. This paper specifies the computing infrastructure used for running experiments (hardware and software), including GPU/CPU models; amount of memory; operating system; names and versions of relevant software libraries and frameworks (yes/partial/no) **partial**
- 4.9. This paper formally describes evaluation metrics used and explains the motivation for choosing these metrics (yes/partial/no) **yes**
- 4.10. This paper states the number of algorithm runs used to compute each reported result (yes/no) **no**
- 4.11. Analysis of experiments goes beyond single-

dimensional summaries of performance (e.g., average; median) to include measures of variation, confidence, or other distributional information (yes/no)  
yes

4.12. The significance of any improvement or decrease in performance is judged using appropriate statistical tests (e.g., Wilcoxon signed-rank) (yes/partial/no)  
yes

4.13. This paper lists all final (hyper-)parameters used for each model/algorithm in the paper's experiments (yes/partial/no/NA) partial

# Supplementary Material

## Derivations and Proofs

### Proof of Limit Formula

Here, we aim to show that as  $t \rightarrow 0$ , the difference between the consistency model outputs converges to the adversarial perturbation, i.e.,  $\mathbf{f}_\theta(\mathbf{z}_t^a, \emptyset, t) - \mathbf{f}_\theta(\mathbf{z}_t, \emptyset, t) \rightarrow \epsilon_a$ .

$$\begin{aligned}
& \lim_{t \rightarrow 0} \mathbf{f}_\theta(\mathbf{z}_t^a, \emptyset, t) - \mathbf{f}_\theta(\mathbf{z}_t, \emptyset, t) \\
&= \lim_{t \rightarrow 0} c_{\text{skip}}(t) \mathbf{z}_t^a + c_{\text{out}}(t) \left( \frac{\mathbf{z}_t^a - \sigma_t \hat{\epsilon}_\theta(\mathbf{z}_t^a, c, t)}{\alpha_t} \right) \\
&\quad - c_{\text{skip}}(t) \mathbf{z}_t - c_{\text{out}}(t) \left( \frac{\mathbf{z}_t - \sigma_t \hat{\epsilon}_\theta(\mathbf{z}_t, c, t)}{\alpha_t} \right) \\
&= \lim_{t \rightarrow 0} c_{\text{skip}}(t) (\mathbf{z}_t^a - \mathbf{z}_t) \\
&\quad + c_{\text{out}}(t) \left( \frac{(\mathbf{z}_t^a - \mathbf{z}_t) - \sigma_t (\hat{\epsilon}_\theta(\mathbf{z}_t^a, c, t) - \hat{\epsilon}_\theta(\mathbf{z}_t, c, t))}{\alpha_t} \right) \\
&= \lim_{t \rightarrow 0} c_{\text{skip}}(t) \sqrt{\bar{\alpha}_t} \epsilon_a + c_{\text{out}}(t) \left( \frac{\sqrt{\bar{\alpha}_t} \epsilon_a - \sigma_t (\hat{\epsilon}_\theta^a - \hat{\epsilon}_\theta)}{\alpha_t} \right) \\
&= \lim_{t \rightarrow 0} c_{\text{skip}}(t) \sqrt{\bar{\alpha}_t} \epsilon_a \\
&= \epsilon_a
\end{aligned} \tag{19}$$

### Derivation of Equation (10)

In Equation (9), our objective is to select  $k_t$  such that the adversarial perturbation  $\epsilon_a$  is effectively removed, given that only the adversarial latent  $\mathbf{z}^a$  is available at inference. Following (Dhariwal and Nichol 2021), we leverage Bayes' theorem and the properties of Gaussian distributions to rewrite the sampling formulation as:

$$\begin{aligned}
q(\tilde{\mathbf{z}}_{t-1} | \tilde{\mathbf{z}}_t, \mathbf{z}_0) &= \frac{q(\mathbf{z}_0, \tilde{\mathbf{z}}_{t-1}, \tilde{\mathbf{z}}_t)}{q(\mathbf{z}_0, \tilde{\mathbf{z}}_t)} \\
&= q(\tilde{\mathbf{z}}_t | \tilde{\mathbf{z}}_{t-1}, \mathbf{z}_0) \frac{q(\tilde{\mathbf{z}}_{t-1} | \mathbf{z}_0)}{q(\tilde{\mathbf{z}}_t | \mathbf{z}_0)} \\
&\propto \exp \left( -\frac{1}{2} \left( \mathbf{A} (\tilde{\mathbf{z}}_{t-1})^2 + \mathbf{B} \tilde{\mathbf{z}}_{t-1} + \mathbf{C} \right) \right)
\end{aligned} \tag{20}$$

where,

$$\begin{aligned}
\mathbf{A} &= \frac{1 - \bar{\alpha}_t}{(1 - \alpha_t)(1 - \bar{\alpha}_{t-1})} \\
\mathbf{B} &= -2\sqrt{\alpha_t} \cdot \frac{\tilde{\mathbf{z}}_t - (\sqrt{\alpha_t} k_{t-1} - k_t) \epsilon_a}{1 - \alpha_t} \\
&\quad - 2 \frac{\sqrt{\bar{\alpha}_{t-1}} \mathbf{z}_0 + (\sqrt{\bar{\alpha}_{t-1}} - k_{t-1}) \epsilon_a}{1 - \bar{\alpha}_{t-1}}
\end{aligned} \tag{21}$$

To achieve our goal, we should remove terms related to  $\epsilon_a$  in Equation (20), which leads to:

$$\frac{\sqrt{\alpha_t} (\sqrt{\alpha_t} k_{t-1} - k_t) \epsilon_a}{1 - \alpha_t} = \frac{(\sqrt{\bar{\alpha}_{t-1}} - k_{t-1}) \epsilon_a}{1 - \bar{\alpha}_{t-1}} \tag{22}$$

Then we have:

$$\begin{aligned}
k_t &= \frac{\bar{\alpha}_t - 1}{\sqrt{\alpha_t} (\bar{\alpha}_{t-1} - 1)} k_{t-1} + \frac{\sqrt{\bar{\alpha}_{t-1}} (1 - \alpha_t)}{\sqrt{\alpha_t} (\bar{\alpha}_{t-1} - 1)} \\
&= \frac{\sqrt{\alpha_t} (\bar{\alpha}_t - 1)}{\bar{\alpha}_t - \alpha_t} k_{t-1} + \frac{\sqrt{\bar{\alpha}_{t-1}} (1 - \alpha_t)}{\bar{\alpha}_t - \alpha_t}
\end{aligned} \tag{23}$$

By dividing both sides by  $\sqrt{\bar{\alpha}_t}$ , we obtain the recursive formula:

$$\frac{k_t}{\sqrt{\bar{\alpha}_t}} = \frac{\bar{\alpha}_t - 1}{\bar{\alpha}_t - \alpha_t} \frac{k_{t-1}}{\sqrt{\bar{\alpha}_{t-1}}} + \frac{1 - \alpha_t}{\bar{\alpha}_t - \alpha_t} \tag{24}$$

Thus, we can easily obtain the closed-form expression:

$$\frac{k_t}{\sqrt{\bar{\alpha}_t}} = \frac{\bar{\alpha}_1 (1 - \bar{\alpha}_t)}{\bar{\alpha}_t (1 - \bar{\alpha}_1)} \left( \frac{k_1}{\sqrt{\bar{\alpha}_1}} - 1 \right) + 1 \tag{25}$$

With  $k_T = 0$ , replace  $t = T$  in the equation, we have:

$$\frac{k_1}{\sqrt{\bar{\alpha}_1}} = 1 - \frac{\bar{\alpha}_T (1 - \bar{\alpha}_1)}{\bar{\alpha}_1 (1 - \bar{\alpha}_T)} \tag{26}$$

Finally we can obtain the closed-form expression of  $k_t$ :

$$k_t = \sqrt{\bar{\alpha}_t} \left( 1 - \frac{\bar{\alpha}_T (1 - \bar{\alpha}_t)}{\bar{\alpha}_t (1 - \bar{\alpha}_T)} \right) = \sqrt{\bar{\alpha}_t} - \frac{\bar{\alpha}_T (1 - \bar{\alpha}_t)}{\sqrt{\bar{\alpha}_t} (1 - \bar{\alpha}_T)} \tag{27}$$